Supporting Information

Serr et al. 10.1073/pnas.1606646113

SI Materials and Methods

Antibodies for Flow Cytometry. The following monoclonal antibodies were used for human FACS staining: anti-CD45RO allophycocyanin (APC)-H7 (UCHL1), anti-CD4 V500 (RPA-T4), anti-PD1 peridinin chlorophyll protein (PerCP)-Cy5.5 (EH12.1), and anti-CD45 APC-H7 (2D1) (all from BD Biosciences) and anti-CD45RA FITC (HI100), anti-CD8a Pacific Blue (RPA-T8), anti-CD11b Pacific Blue (ICRF44), anti-CD14 Pacific Blue (HCD14), anti-CD19 Pacific Blue (HIB19), anti-CCR7 PE-Cy7 (G043H7), anti-CXCR5 APC (J252D4), anti-CD3 Alexa Fluor 700 (HIT3a), anti-CXCR3 APC-Cy7 (G025H7), anti-CXCR3 PerCP-Cy5.5 (G025H7), anti-CCR6 PE-Cy7 (G034E3), anti-ICOS PE (C398.4A), anti-PSGL1 PE (KPL-1), anti-CD20 FITC (2H7), and anti-CD27 APC (M-T271) (all from Biolegend). For murine FACS staining, the following monoclonal antibodies were used: anti-CD4 Biotin (GK1.5), anti-CD14 BD Horizon 450 (rmC5-3), and anti-Bcl6 Alexa Fluor 647 (K112-91) (all from BD Biosciences); anti-CD44 PE (IM7), anti-CD25 PerCP-Cy5.5 (PC61), anti-ICOS FITC (C398.4A), anti-CXCR5 PerCP-Cy5.5 (L138D1), anti–PD-1 Alexa Fluor 780 (J43), anti-CD4 Alexa Fluor 700 (RM4-5), anti-CD8a Pacific Blue (53-6.7), anti-CD11b Pacific Blue (M1/70), anti-B220 Pacific Blue (RA3-6B2), anti-F4/80 Pacific Blue (BM8), and anti-CD11c Brilliant Violet 421 (N418) (all from Biolegend); and anti-CCR7 PE (4B12) and anti-Foxp3 FITC (FJK-16s) (both from eBiosciences).

Primers. For RT-qPCR analysis of gene expression, the following primers were used: QuantiTect Primer Assays (Qiagen) for IFN-γ, IL-13, IL-10, CXCR5, ICOS, ITCH, Bcl6, KLF2, PTEN, Foxo1, S1P1R, PHLPP2, and CTLA4 and PrimePCR PreAmp for SYBR Green Assay (BioRad) for Ascl2, IL-17a, and IL-4. The sequence for the primers for ICOS is as follows: forward (Fwd): GCA CGA CCC TAA CGG TGA AT and reverse (Rev): GAA AAC TGG CCA ACG TGC TT, and the sequence for the primers for IL-21 is as follows: Fwd: CTC CCA AGG TCA AGA TCG CC and Rev: TGG CAG AAA TTC AGG GAC CA.

Chitosan-Coated PLGA Nanoparticle Preparation and Characterization. The nanoparticles were produced following the method described by Ravi Kumar et al. (39) using PLGA Resomer RG 752H (Evonik) and Protasan UP CL 113 Chitosan (NovaMatrix). For confocal imaging, the nanoparticles were produced with a 5-fluorescineamine (FA)-PLGA conjugate. The measured hydrodynamic diameter was 146.7 ± 0.8 nm (152.8 ± 1.2 nm), the polydispersity index was 0.068 ± 0.009 (0.056 ± 0.007), and the zeta potential was +29.6 ± 0.3 mV (+29.6 ± 0.7 mV) for the chitosan-coated PLGA nanoparticles and FA-labeled nanoparticles.

Analysis of miRNA/Nanoparticles Uptake by Confocal Imaging of $CD4^+$ T-Cell Cytospins. Chitosan-coated PLGA nanoparticles (~130 nm in size) with or without fluorescent label (FA) were obtained from Claus-Michael Lehr at the Department of Drug Delivery, Helmholtz Institute for Pharmaceutical Research Saarland, Saarland University, Germany. Successful uptake and delivery of miRNA to human and murine $CD4^+$ T cells was determined: Respective naive $CD4^+$ T cells were stimulated with anti-CD3/anti-CD28 for 18 h in the presence of FA-labeled nanoparticles complexed with miRIDIAN miRNA transfection control (Dy547). The uptake was initially confirmed by identification of a clearly distinguishable FA^+ population using FACS analysis. Additionally the uptake was confirmed by confocal imaging: Human naive $CD4^+$ T cells were stimulated as described above for 18 h in the presence or absence of nanoparticles and labeled miRIDIAN miRNA mimic transfection control (Dy547). After the stimulation, $CD4^+$ T cells were washed and fixed. Upon generation of cytospins, intracellular localization of nanoparticles and delivered miRNA were assessed by confocal microscopy.

Insulin Autoantibody Assay. Insulin autoantibodies were determined using an ELISA system as described previously. In brief, high-binding, 96-well plates (Costar) were coated with human recombinant insulin (10 μg/mL; Sigma–Aldrich) overnight at 4 °C. Unspecific blocking was done using PBS containing 2% BSA for 2 h at room temperature. Preincubated serum (diluted 1:10) with or without insulin competition was added and incubated for 2 h at room temperature. After four wash steps, biotinylated anti-mouse IgG1 (Abcam) diluted 1:10,000 in PBS/BSA was added for 30 min at room temperature. After washing the plate, horseradish peroxidase-labeled streptavidin was added for 15 min. The plate was washed five times, and tetramethylbenzidine (TMB) substrate solution was added (OptEIA reagent set; Becton, Dickinson and Company). The reaction was stopped using sulfuric acid, and fluorescent intensity was determined in the Epoch plate reader (Biotech). Each sample was run in duplicate with and without competition using human insulin. For each sample, an index was calculated based on the mean of the results.

To determine levels of IAA in NOD mice, a Protein A/G radiobinding assay based on ^{125}I-labeled recombinant human insulin was applied as previously described (62). Serum from non-autoimmune prone BALB/c mice was used as negative control.

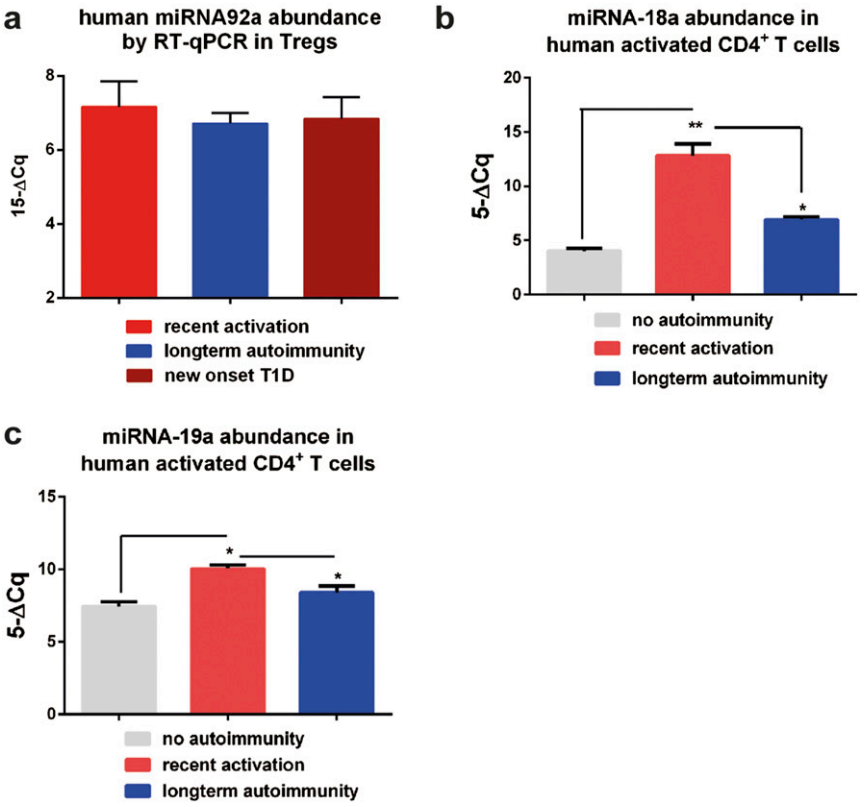

Fig. S1. (*A*) miRNA92a abundance in $CD4^+CD3^+CD127^{low}CD25^{high}$ Treg cells. miRNA18a (*B*) and miRNA19a (*C*) abundance in human $CD4^+$ T cells purified from children with or without pre-T1D (no autoimmunity, $n = 10$; recent onset of autoimmunity, $n = 6$; long-term autoimmunity, $n = 6$) as assessed by qRT-PCR analyses. Data represent the mean ± SEM. $^*P < 0.05$; $^{**}P < 0.01$.

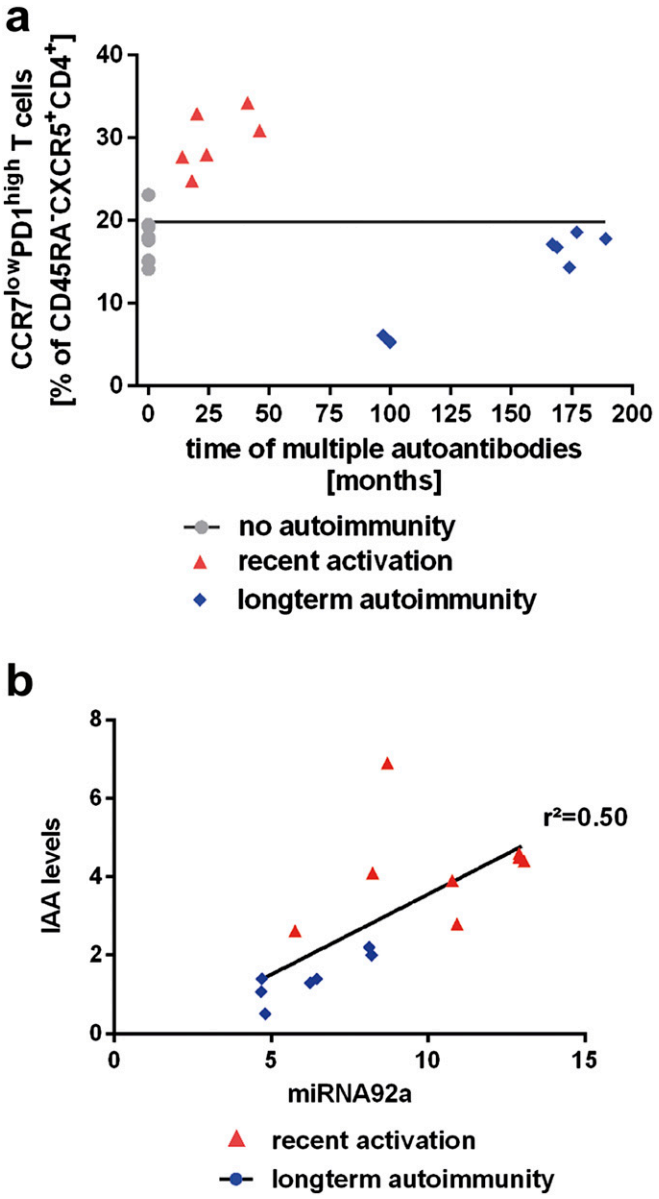

Fig. S2. (*A*) Correlation of duration of islet autoimmunity (months of multiple islet autoantibody positivity) with $CXCR5^{+}CCR7^{low}PD1^{high}CD4^{+}$ T cells. (*B*) Correlation of miRNA92a abundance in $CD4^{+}$ T cells with IAA levels in serum.

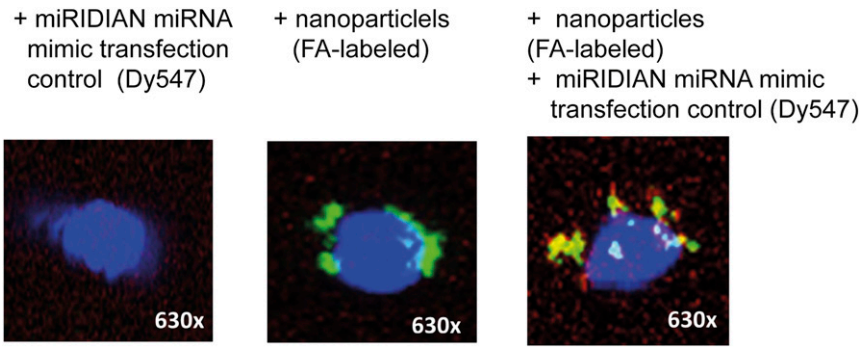

Fig. S3. Assessment of uptake, intracellular colocalization of FA-labeled nanoparticles, and Dy457-labeled transfection control miRNA mimic in $CD4^{+}$ T cells upon stimulation with anti-CD3/anti-CD28 by confocal microscopy.

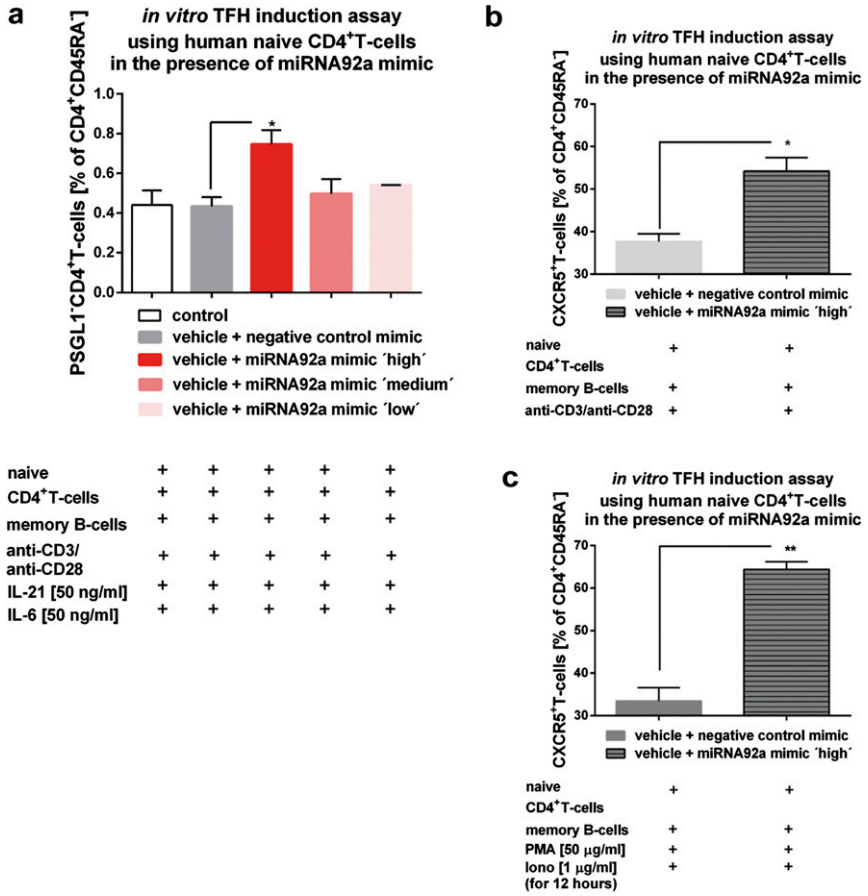

Fig. S4. (*A*) TFH precursor induction using human naive $CD4^+$ T cells in the presence of memory B cells and IL-6, IL-21, and a titration of a miRNA92a mimic (low = 0.0375 μg in 200 μL per 100,000 cells, medium = 0.075 μg in 200 μL per 100,000 cells, and high = 0.15 μg in 200 μL per 100,000 cells) or a negative miRNA mimic control. Summary graph for frequencies of $PSGL1^-CD4^+$ T cells is shown as percentages of $CD4^+CD45RA^-$ T cells ($n = 4$). Data represent the mean ± SEM from duplicate wells per individual. $^*P < 0.05$. (*B*) TFH precursor induction using human naive $CD4^+$ T cells in the presence of memory B cells and a miRNA92a mimic or a negative miRNA mimic control. Summary graph for frequencies of $CXCR5^+CD4^+$ T cells is shown as percentages of $CD4^+CD45RA^-$ T cells ($n = 4$). Data represent the mean ± SEM from duplicate wells per individual. $^*P < 0.05$. (*C*) TFH precursor induction using human naive $CD4^+$ T cells in the presence of memory B cells and a miRNA92a mimic or a negative miRNA mimic control. In such assays, PMA (50 ng/mL) and ionomycin (1 μg/mL) were added for the last 12 h of the experiments, and frequencies of $CXCR5^+CD4^+$ T cells shown as percentages of $CD4^+CD45RA^-$ T cells were analyzed ($n = 4$). Data represent the mean ± SEM from duplicate wells per individual. $^{**}P < 0.01$.

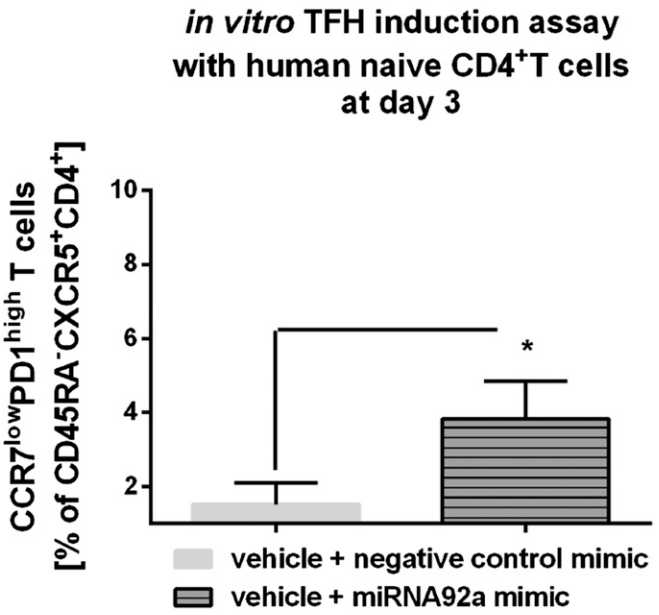

Fig. S5. TFH precursor induction using human naive $CD4^+$ T cells in the presence of memory B cells with or without a miRNA92a mimic or respective negative control mimics. Summary graphs are shown for frequencies of $CCR7^{low}PD1^{high}$ cells presented as percentages of $CXCR5^+CD45RA^-CD4^+$ T cells after a 3-d culture. Data represent the mean ± SEM. $^*P < 0.05$.

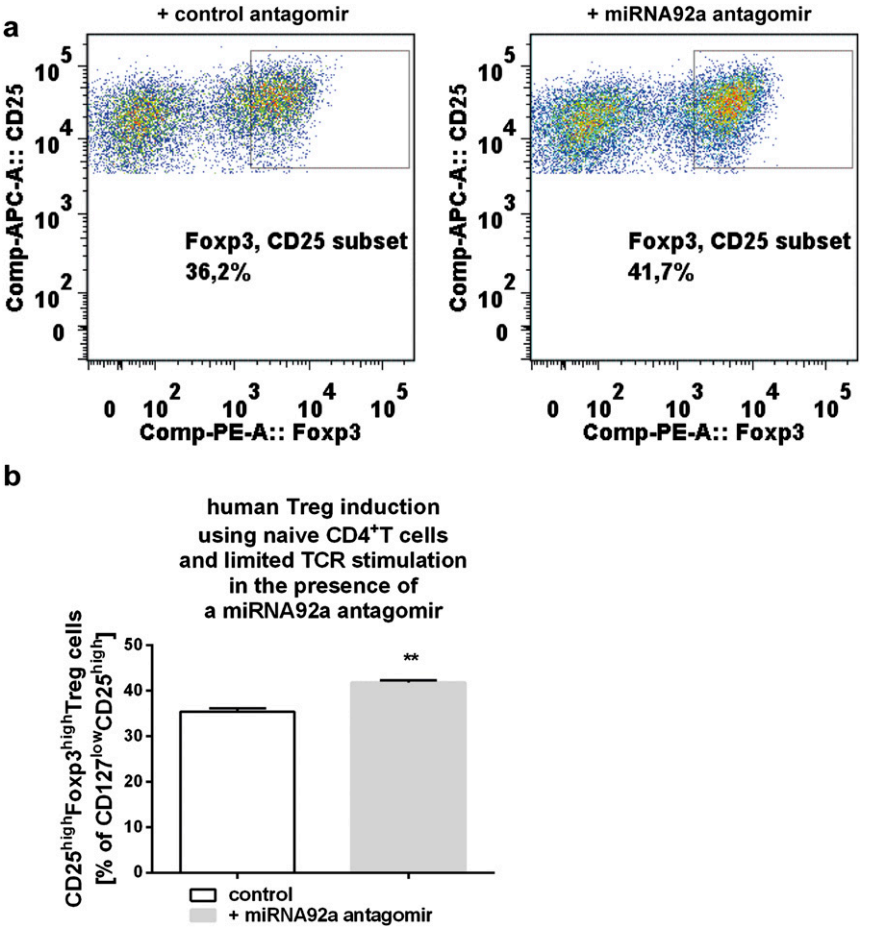

Fig. S6. (*A*) Human Treg-cell induction using human naive $CD4^+$ T cells in the presence of a miRNA92a antagomir (0.075 μg in 200 μL per 100,000 cells) or respective negative control antagomir and limited T-cell receptor stimulation. (*B*) Summary graph for frequencies of induced human $CD127^{low}CD25^{high}$ $Foxp3^{high}$ Treg cells ($n = 4$). Data represent the mean ± SEM from triplicate wells. $^{**}P < 0.01$.

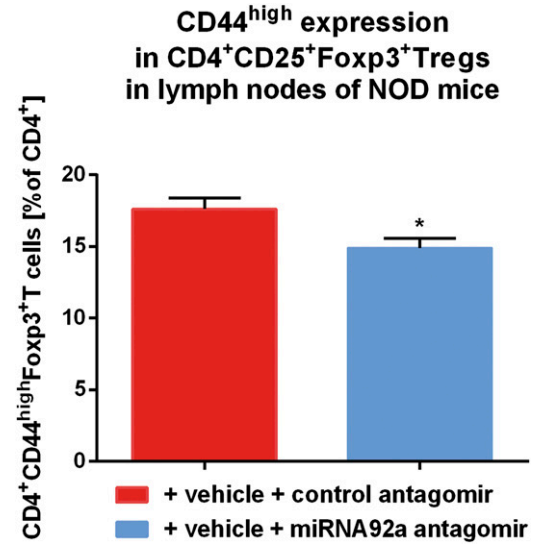

Fig. S7. Summary graph for CD44^{high} expression in CD4^{+}CD25^{+}Foxp3^{+} Treg cells purified from lymph nodes of NOD mice given a control antagomir or a miRNA92a antagomir (14 d of treatment, with injections four times per week at 5 mg/kg) ($n = 5$ per group). Data represent the mean ± SEM. *$P < 0.05$.

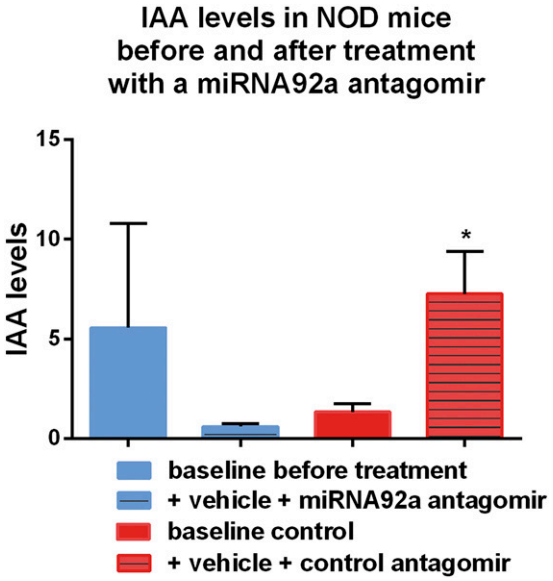

Fig. S8. Summary graphs for IAA levels from NOD mice before and after treatment with either control antagomirs or a specific miRNA92a antagomir (14 d of treatment, with injections four times per week at 5 mg/kg) ($n = 5$ per group). Data represent the mean ± SEM. *$P < 0.05$.

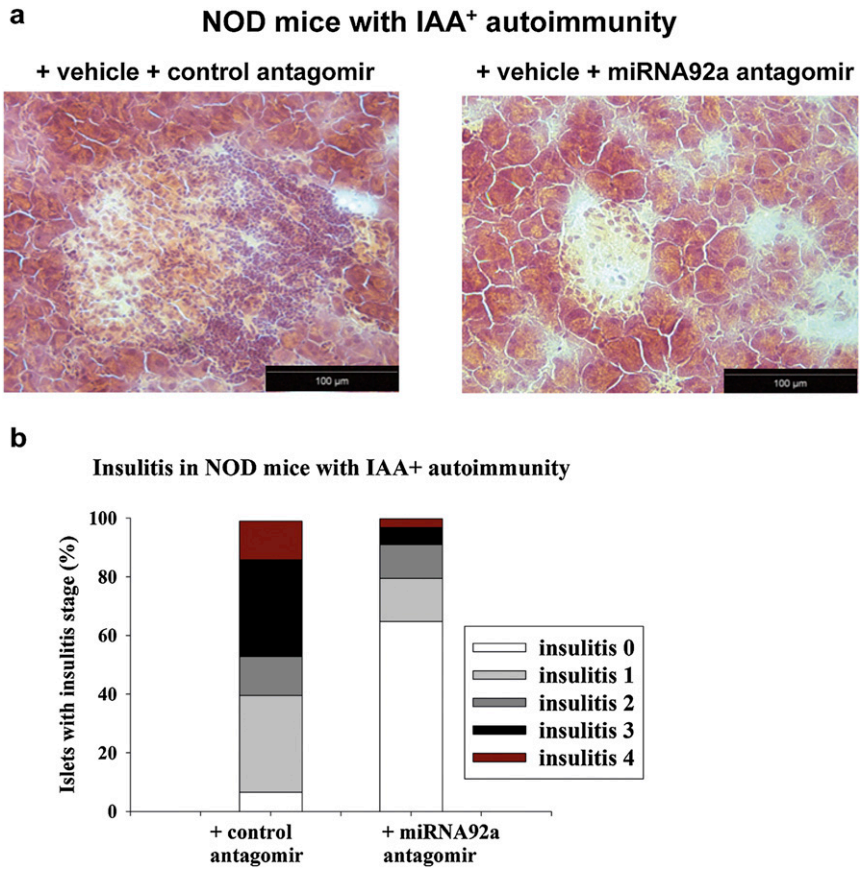

Fig. S9. (*A*) Histopathological evaluation of pancreas sections from NOD mice with IAA$^+$ autoimmunity that were given a control antagomir or a miRNA92a antagomir (14 d of treatment, with injections four times per week at 5 mg/kg). Representative hematoxylin and eosin-stained pancreas cryosections are shown. (*B*) Grading of insulitis from NOD mice as in *A* (n = 5 per group).

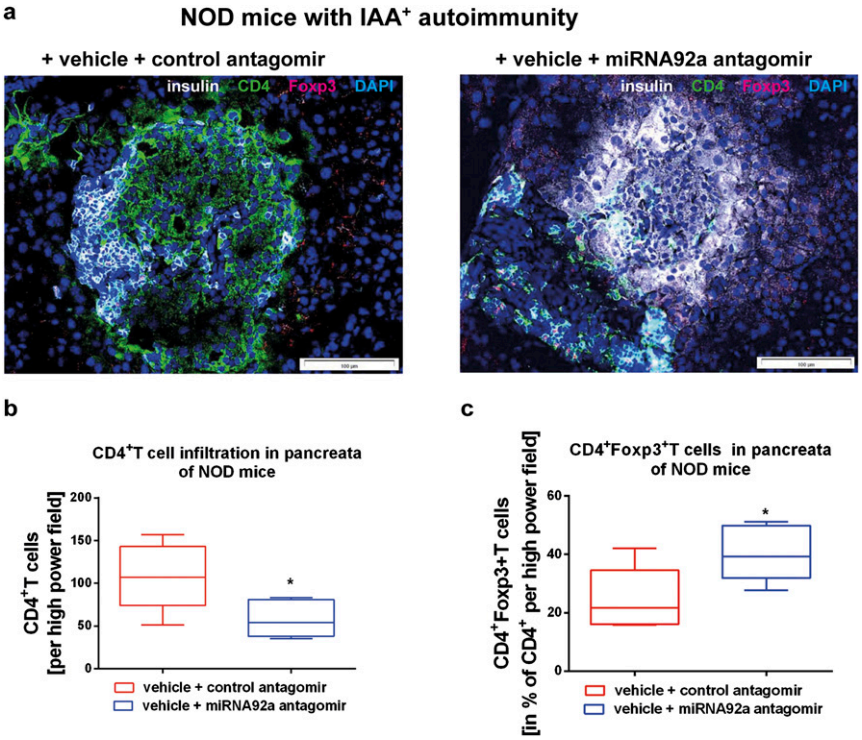

Fig. S10. (*A*) Immunofluorescence for insulin (white), CD4 (green), and Foxp3 (red) in pancreatic cryosections of NOD mice given a control inhibitor or a miRNA92a inhibitor (14 d of treatment, with injections four times per week at 5 mg/kg). (*B*) $CD4^+$ T cells infiltrating the pancreas as in *A*. Shown are box and whiskers plots of $CD4^+$ T cells per high-power field. (*C*) $CD4^+Foxp3^+$ T cells in the percentage of infiltrating $CD4^+$T cells per high-power field of mice as in *A* (n = 5 per group).